Since January 2020 Elsevier has created a COVID-19 resource centre with free information in English and Mandarin on the novel coronavirus COVID-19. The COVID-19 resource centre is hosted on Elsevier Connect, the company's public news and information website.

Journal of Molecular Structure 1246 (2021) 131166

Contents lists available at ScienceDirect

Journal of Molecular Structure

journal homepage: www.elsevier.com/locate/molstr

The iron(III) and nickel(II) complexes with tetradentate thiosemicarbazones. Synthesis, experimental, theoretical characterization, and antiviral effect against SARS-CoV-2

Belkis Atasever Arslan[a,*], Büşra Kaya[b], Onur Şahin[c], Sefer Baday[d], Cemil Can Saylan[d], Bahri Ülküseven[b]

[a] Department of Molecular Biology and Genetics, Faculty of Engineering and Natural Sciences, Üsküdar University, Istanbul, Turkey
[b] Department of Chemistry, Engineering Faculty, Istanbul University-Cerrahpasa, 34320 Avcilar, Istanbul, Turkey
[c] Scientific and Technological Research Application and Research Center, Sinop University, 57000, Sinop, Turkey.
[d] Applied Informatics Department, Informatics Institute, Istanbul Technical University, Istanbul, Turkey

ARTICLE INFO

Article history:
Received 6 May 2021
Revised 14 July 2021
Accepted 21 July 2021
Available online 22 July 2021

Keywords:
Iron
Nickel
Thiosemicarbazone
SARS-CoV-2

ABSTRACT

The discovery of new inhibitors that can be used in the treatment of viral diseases, including Covid-19, is an area open to research, and there is a need for innovative compounds with increased efficiency that provide inhibition by suppressing enzyme, and receptor mechanisms. The iron(III) and nickel(II) complexes were synthesized by template condensation of 4-methoxy-salicylaldehyde with S-methylthiosemicarbazone derivatives of 1,1,1-trifluoroacetylacetone (for **Fe1**) and methylacetoacetate (for **Ni1**). The complex structures having N_2O_2-chelating thiosemicarbazidato ligand were identified by analytical, spectroscopic, and X-ray crystallography results. Coordination environment of iron(III) center in complex **Fe1** has a distorted square pyramidal geometry consisting of the N_2O_2 donor set and a chlorine atom, while that of **Ni1** is square plane with the set. Inhibitory effect of **Fe1** compound against SARS-CoV-2 virus specific 3C-like protease enzyme was investigated experimentally. It was determined that the highest inhibition concentration of **Fe1** was 100 μM. Percent inhibition activity at this concentration was on average 30.62 $\pm$ 3.809%. Binding of both compounds to the 3C-like protease enzyme specific to the SARS-CoV-2 virus was analyzed using docking calculations. As a result of the docking calculation of **Fe1**, it has been observed that the compound has a binding energy of -7.4 kcal / mol to 3CL-like protease. It has been observed that the protein amino acids GLY143, THR26, and ASN142 contribute to the high binding affinity of the **Fe1**. The experimental and theoretical results obtained for the two complexes support each other.

1. Introduction

Thiosemicarbazone chemistry is an expanding topic by participation of their transition metal complexes having drug potential [1–6]. For pharmacological purposes, even though platinum, palladium and copper ions are mostly preferred in complex formations of thiosemicarbazones, iron(III) and nickel(II) have also been included in studies in recent years [7–10].

Metal complexes of S-alkylthiosemicarbazones with salen-like donor atom set (N_2O_2) have been exhibited remarkable potentials as anti-cancer drug active ingredients. In an *in vitro* study, a series of palladium(II) complexes obtained from acetylacetone-S-alkyl thiosemicarbazones were reported to have much lower IC_{50} values than cisplatin on HepG2 and Hep3B hepatocellular carcinomas, HCT116 colorectal carcinoma cells [6]. This performance has been associated with their xanthine oxidase inhibitions between 0.42 - 12.01 μg/ml of IC_{50} values. Remarkable cytotoxicity data were obtained also with the iron(III) and nickel(II) complexes containing this type of tetradentate thiosemicarbazones [7,9,10]. An iron(III) complex with a tetradentate S-methylthiosemicarbazidato ligand showing a meaningful cytotoxic effect against HT-29 and HeLa cell lines was found to be linked to CT-DNA with intercalation mode and calculated its intrinsic DNA-binding constant (K_b) as 1×10^5 M^{-1} from data of the experiments performed with calf thymus DNA [11]. Moreover, enzyme inhibition capabilities [6], antidiabetic [12] and antioxidant properties [13–15] of metal complexes with N_2O_2-thiosemicarbazone ligands have been reported.

* Corresponding author.
E-mail address: belkisatasever.arslan@uskudar.edu.tr (B. Atasever Arslan).

https://doi.org/10.1016/j.molstruc.2021.131166
0022-2860/

The 2019 coronavirus disease outbreak (COVID-19) caused by severe acute respiratory syndrome coronavirus 2 (SARS-CoV-2) has resulted in more than 3 million deaths in less than a year. SARS-CoV-2 infection has a wide range of clinical manifestations, including both asymptomatic cases and rapid deaths [16]. Activation of the immune system and production of inflammatory cytokines are essential for natural anti-viral immune responses [17]. However, hyperactivation of the immune system causes an acute increase in circulating pro-inflammatory cytokine levels, leading to a "cytokine burst" [18]. Cytokine burst is clinically characterized by systemic inflammation, hyperferritinemia, hemodynamic instability, and multi-organ failure [19].

The transition metal complexes of thiosemicarbazones show various biological activities and have been the subject of many studies [20–26]. In addition to these studies, which mostly focus on the search for cancer-preventing active substances, there are also studies examining antiviral effects. Frequently, thiosemicarbazones have been studied as organic molecules in antiviral property studies, and metal complexes are few in number. In a study in which platinum(II) and palladium(II) complexes of thiophene-2-carboxaldehyde thiosemicarbazone derivatives were examined, activity against DNA and RNA viruses was investigated [27]. Complexes of the same metals with pyridine-2-carbaldehyde thiosemicarbazone exhibited considerable efficacy against herpes simplex virus 1 (HSV-1) [28]. In another study; The efficiency of thiosemicarbazones copper(II) and nickel(II) complexes against HIV viruses has been determined [29].

The biological activity potential of metal complexes of such N_2O_2-chelating thiosemicarbazone ligands have been known since 2007 [30]. An iron and a nickel(II) centered complexes bearing such thiosemicarbazones were synthesized and structurally defined. In the study, the inhibitory effects of the two compounds against SARS-CoV2 3CL-like protease were investigated considering the enzyme inhibition abilities and the antiviral effect potentials of thiosemicarbazone compounds. The virus contains four non-structural proteins: papain-like (PLpro) and 3-chymotrypsin-like (3CLpro) proteases, RNA polymerase and helicase. Both proteases (PLpro and 3CLpro) are involved in transcription and replication of the virus. Among the four proteins, 3CLpro is mainly involved in the replication of the virus [31]. One of the main target proteins in inhibiting virus replication is 3CL main protease enzyme. In the study, first, the binding affinity of the substances against the 3CL main protease enzyme by autodocking was examined, and then the inhibitory effect of the **Fe1** substance with high binding affinity was experimentally investigated.

2. Materials and methods

2.1. Apparatus and methods

The elemental analyses were determined on a Thermo Finnigan Flash EA 1112 Series Elemental Analyzer. IR spectra were obtained using ATR unit on Agilent Carry 630 spectrophotometer. ^{1}H NMR spectra were measured on Varian UNITY INOVA 500 MHz NMR spectrometer. UV-Visible spectra were recorded on Ocean Optics QE65000 diode array spectrophotometer. Magnetic moment measurements were carried out by Gouy technique with an MK I model device of Sherwood Scientific at room temperature.

Suitable crystals of **Fe1** and **Ni1** were selected for data collection which was performed on a Bruker D8-QUEST diffractometer equipped with a graphite-monochromatic Mo-Kα radiation at 296 K. The H atoms were located from different maps and then treated as riding atoms with C-H distances of 0.93-0.96 Å. We used these procedures for our analysis: solved by direct methods; SHELXS-2013 [32]; refined by full-matrix least-squares methods; SHELXL-2013 [33]; data collection: Bruker APEX2 [34]; molecular graphics: MERCURY [35]; solution: WinGX [36]. Powder XRD patterns were recorded by XPERT-PRO diffractometer system using Cu-Kα1 radiation with λ = 1.5406 Å.

2.2. Synthesis

The starting materials, S-methylthiosemicarbazone derivatives of 1,1,1-Trifluoroacetylacetone (**1**) and methylacetoacetate (**2**) were obtained in the form of hydroiodide salt by using literature metods [37–39]. The cream colored reaction products were recrystallized from ethanol-dichloromethane (1:1) and dried *in vacuo*.

(**1**) Yield: 2.58 g, 70.0%; m.p. (°C): 147; Calc. for $C_7H_{11}N_3OSF_3I$ (M_r=369.14), %: C, 22.78; H, 3.00; N, 11.38; S, 13.04. Found, %: C, 22.49; H, 2.83; N, 11.54; S, 12.24. IR (cm^{-1}): $\nu_{as}(NH_2)$ 3354, $\nu_s(NH_2)$ 3249, ν(OH) 3042, $\delta(NH_2)$, ν(C=N) 1642-1541. UV-Vis [in 10^{-5} M $CHCl_3$, λ_{max} (nm), log ε (dm^3 cm^{-1} mol^{-1})]: 242 (5.03), 362 (3.15). ^{1}H NMR (ppm): 9.84 (s, 2H, NH_2), 9.46 (s, 1H, O*H*), 3.70 (s, 2H, -CH_2-), 2.63 (s, 3H, S-CH_3), 2.12 (s, 3H, C-CH_3).

(**2**) Yield: 1.92 g, 58.0%; m.p. (°C): 117; Calc. for $C_7H_{14}N_3O_2SI$ (M_r=331.17), %: C, 25.39; H, 4.26; N, 12.69; S, 9.68. Found, %: C, 25.51; H, 4.03; N, 12.47; S, 9.23. IR (cm^{-1}): $\nu_{as}(NH_2)$ 3260, $\nu_s(NH_2)$ 3165, ν(OH) 3081, $\delta(NH_2)$, ν(C=N) 1722-1574. UV-Vis [in 10^{-5} M $CHCl_3$, λ_{max} (nm), log ε (dm^3 cm^{-1} mol^{-1})]: 241 (5.03), 364 (3.26). ^{1}H NMR (ppm): 9.38 (s, 2H, NH_2), 7.18 (s, 1H, O*H*), 3.65 (s, 3H, O-CH_3), 3.18 (s, 2H, -CH_2-), 2.68 (s, 3H, S-CH_3), 2.22 (s, 3H, C-CH_3).

Monochloro-N^1-1,1,1-Trifluoroacetylacetone-N^4-4-methoxysalicylidene-S-methyl-thiosemicarbazidato iron(III) (**Fe1**)

To a solution of compound **1** (0.37 g, 1.0 mmol) and 4-methoxysalicylaldehyde (0.15 g, 1.0 mmol) in ethanol (10 ml) was added dropwise a solution of $FeCl_3.6H_2O$ (0.27 g, 1.0 mmol) in ethanol (5 ml) and the mixture was stirred at 70°C for 10 min. Then it was cooled to room temperature and Et_3N (0.1 mL) was added to the mixture. After 8 hours a black-looking crystalline product was separated by filtration, washed with 5 mL of ethanol-ether (1:1) and dried *in vacuo* (Fig. 1).

Yield: 0.14 g, 30.0%; m.p. (°C): 310. μ_{eff} (BM): 5.86. Calc. for $C_{15}H_{14}FeClF_3N_3O_3S$ (M_r= 464.64), %: C, 38.77; H, 3.04; N, 9.04; S, 6.90. Found, %: C, 38.56; H, 3.33; N, 8.69; S, 6.37. IR (cm^{-1}): ν(C=N^1) 1615; ν(N^2=C) 1606; ν(N^4=C) 1581; ν(C-O) 1160, 1124. UV-Vis [in 10^{-5} M $CHCl_3$, λ_{max} (nm), log ε (dm^3 cm^{-1} mol^{-1})]: 239 (4.79), 309 (4.98), 422 (4.65)

N^1-methylacetoacetate-N^4-4-methoxysalicylidene-S-methyl-thiosemicarbazidato nickel(II) (**Ni1**)

To a solution of compound **2** (0.33 g, 1.0 mmol) and 4-methoxysalicylaldehyde (0.15 g, 1.0 mmol) in ethanol (10 ml) was added dropwise a solution of $NiCl_2.6H_2O$ (0.24 g, 1.0 mmol) in ethanol (5 ml). The reaction mixture was stirred at 70°C for 10 min. After cooling, 0.1 mL of Et_3N was added to the mixture and allowed to stand at room temperature for 24 h. Red crystalline product was separated by filtration, washed with 5 mL of ethanol ether (1:1) and dried *in vacuo* (Fig. 1).

Yield: 0.14 g, 35.0%; m.p. (°C): 199, μ_{eff} is equal approx. 0 BM. Calc. for $C_{15}H_{17}NiN_3O_4S$ (M_r=394.07), %: C, 45.72; H, 4.35; N, 10.66; S, 8.14. Found, %: C, 45.43; H, 4.64; N, 10.28; S, 7.65. IR (cm^{-1}): ν(C=N^1) 1617; ν(N^2=C) 1591; ν(N^4=C) 1574; ν(C-O) 1149, 1111. UV-Vis [in 10^{-5} M $CHCl_3$, λ_{max} (nm), log ε (dm^3 cm^{-1} mol^{-1})]: 240 (4.99), 262 (4.94), 305 (4.91), 332 (4.84), 341 (4.83), 432 (4.78), 485 (4.59). ^{1}H NMR (ppm): 7.68 (s, 1H, N^4=C*H*), 7.25 (d, 1H, *c*), 6.55 (s, 1H, *a*), 6.38 (d, 1H, *b*), 4.62 (s, 1H, =C*H*), 3.83 (s, 3H, OCH_3), 3.79 (s, 3H, OCH_3), 2.60 (s, 3H, S-CH_3), 2.28 (s, 3H, C-CH_3).

2.3. Docking calculations

In the study, binding pose and affinity of both compounds to the 3C-like protease enzyme specific to the SARS-CoV-2 virus were

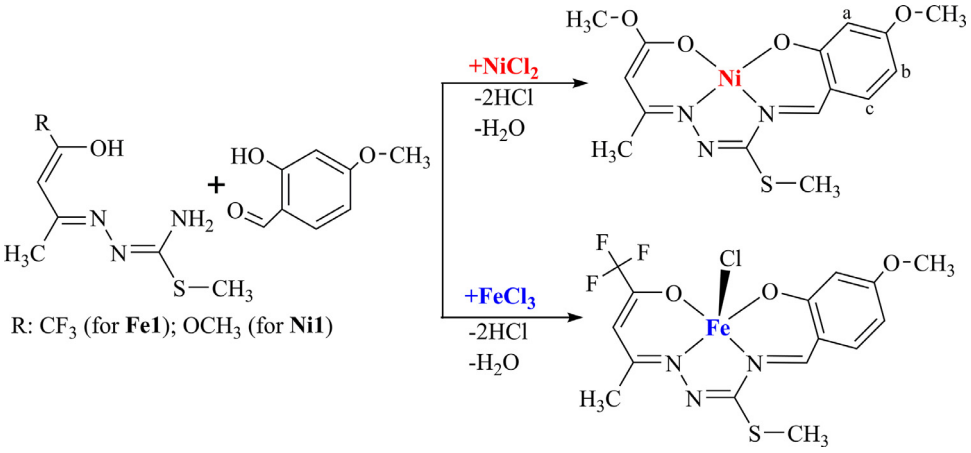

Fig. 1. Synthesis scheme of the complexes.

analyzed via molecular docking study using AutoDock VINA package [40]. In the docking calculation, 3C-like protease structure was taken from the Protein Data Bank (PDB code 6LU7). The protonation of residues was calculated at pH 7 using PROPKA [41]. The grid box was centered to the previously defined binding pocket, and the box size was set to 24 Å for each axis [42]. First, rigid docking procedure was followed. Next, flexible docking was carried out with the same grid box and size parameters. In the flexible docking, the side chain of residues THR25, HIS41, MET49, GLN142, and GLN189 were specified as flexible.

2.4. SARS-CoV2 3CL protease activity assay

The inhibitory activity of complex **Fe1** compound, which shows high binding affinity against the SARS-CoV-2 virus-specific 3C-like protease enzyme according to the auto-docking results, was also examined with the commercially available BPS Bioscience 3CL Protease assay kit (Catalog # 79955). Experiments were made according to manufacturer's protocol. To understand inhibition percent of **Fe1**, its 0.1, 0.5, 25, 100 μM concentrations were used. **Fe1** was dissolved in DMSO and a 10 mM stock solution was prepared. Its 0.1, 0.5, 25, 100 μM concentrations were prepared 3CL protease assay buffer included BPS Bioscience 3CL Protease assay kit. Concentrations were created so that there would be no more than 1% DMSO. 3CL protease assay buffer with the same amount of DMSO was analyzed as a control. Absorbance values of the controls subtracted from other wells. GC376 included in the kit was used as inhibitor control. The inhibition level of the substances was analyzed by comparing with GC376.

3. Results and Discussion

3.1. Structural characterization

The template condensation of the starting materials (**1** and **2**) with 4-methoxysalicylaldehyde in the presence of nickel(II) or iron(III) in the 1:1:1 molar ratio yielded the solid complexes. The formation and purity of the complexes were confirmed by elemental analysis, IR, UV-Vis and ^{1}H NMR spectra (for **Ni1**) as well as single crystal X-ray diffraction analysis (Figure S1-S4). The $\nu(NH_2)$, ν(OH), and also $\delta(NH_2)$ bands disappeared in the infrared spectra of the complexes due to reactions of hydroxy and thioamide groups on **1** and **2**. Similarly, no signals of the OH and NH_2 groups were observed in the ^{1}H NMR spectra of complex **Ni1** (Figure S3). The resulting N^4=CH and C=CH signals which are singlets and equivalent to the integral value of one proton, confirmed the chelate formation around nickel(II). The spectra showed the expected chemical shift values of the protons belonging to O-CH_3, S-CH_3 and C-CH_3 groups in addition to the aromatic protons in the range of 7.25-6.38 ppm.

The electronic spectrum of the complexes showed $\pi \rightarrow \pi^*$ and $n \rightarrow \pi^*$ bands, which are transitions due to imine, thioamide groups and the phenyl ring, in the range of 239-341 nm. The bands recorded at 432 and $485_{(shoulder)}$ nm for **Ni1** and 422 nm for **Fe1** can be assigned to charge transfer transitions. Because of quite low intensities, *d–d* transitions belonging to both complexes could be not observed in the spectra.

The μ_{eff} value of **Fe1** (5.86 BM) indicates the five unpaired d^5 structure. Magnetic measurement result of **Ni1** shows diamagnetic form that is attributed to square-planar structure.

3.2. Crystallography

The molecular structures of **Fe1** and **Ni1**, with the atom numbering schemes, are shown in Fig. 2. In **Fe1**, the iron(III) ion is coordinated by two oxygen atoms [Fe1-O1=1.897(2) Å and Fe1-O3=1.907(2) Å] and two nitrogen atoms [Fe1-N1=2.067(3) Å and Fe1-N3=2.076(3) Å] from thiosemicarbazone ligand and chlorine atom [Fe1-Cl1=2.2146(11) Å]. The geometry of the Fe1 atom can be evaluated by the Addison distortion index tau ($\tau = (\beta-\alpha)/60$, where α and β are the two largest coordinated angles in the complex). In a five-coordinate geometry, $\tau = 0$ for a square pyramidal geometry and τ=1 for a trigonal bipyramidal geometry. The τ value is calculated as 0.05 and this value shows that Fe1 atom has a distorted square pyramidal geometry (Table 1). In **Fe1** crystal, atom C4 in the molecule at (x, y, z) acts as hydrogen-bond donor to the one of flour atoms in molecule at (x, y, z+1), so forming a C(11) chain which is running parallel to the [001] direction (Figure S1a, S2).

Tables 2 and 3.

In the nickel(II) complex, the metal center is coordinated by two oxygen atoms [Ni1-O1=1.842(5) Å and Ni1-O3=1.873(5) Å] and two nitrogen atoms [Ni1-N1=1.842(6) Å and Ni1-N3=1.839(6) Å] of the ligand backbone, thus showing a distorted square planar coordination geometry. The C4 atom in the **Ni1** molecule at (x, y, z) acts as hydrogen-bond donor to the O4 atom in the molecule at (x+1, y+1, z), so forming a C(10) chain which is running parallel to the [110] direction (Figure S1b, S2).

3.3. X-ray powder diffraction

The powder XRD diffraction is carried out for complexes **Fe1** and **Ni1** which shows prominent sharp peaks, with the evaluating

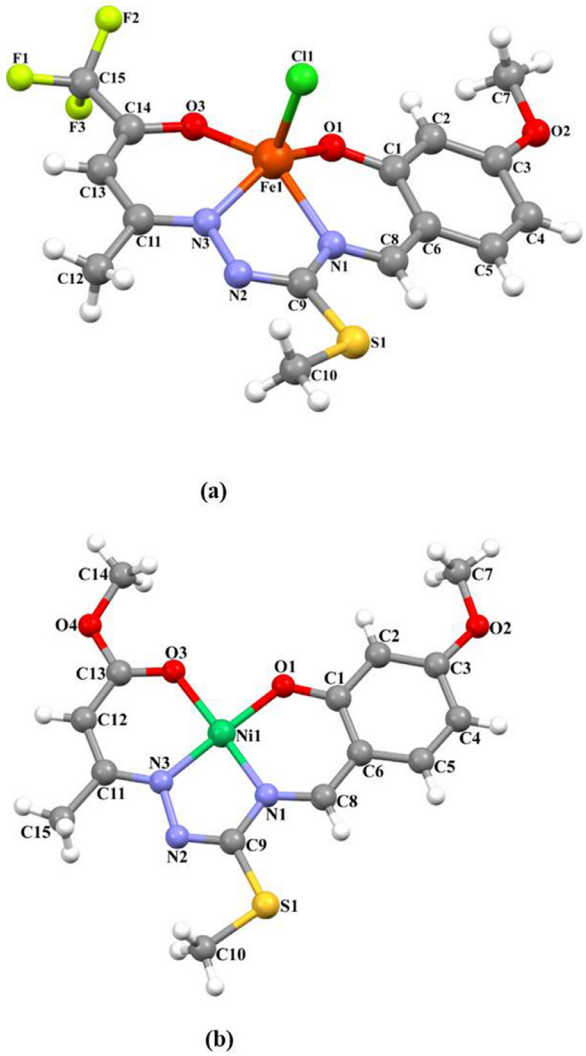

Fig. 2. The molecular structures of **Fe1** (**a**) and **Ni1** (**b**) showing the atom numbering schemes.

Table 1
Crystal data and structure refinement parameters for **Fe1** and **Ni1**.

	Fe1	Ni1
Empirical formula	$C_{15}H_{14}ClF_3FeN_3O_3S$	$C_{15}H_{17}N_3NiO_4S$
Formula weight	464.65	394.08
Crystal system	Triclinic	Triclinic
Space group	P-1	P-1
a (Å)	8.1510 (6)	4.8494 (6)
b (Å)	9.2058 (7)	11.8570 (16)
c (Å)	13.3198 (10)	15.331 (2)
α (°)	85.271 (3)	106.763 (6)
β (°)	74.269 (4)	96.289 (5)
γ (°)	80.017 (3)	99.336 (6)
V (Å^3)	946.81 (12)	821.42 (19)
Z	2	2
Diffractometer	BRUKER D8-QUEST	
Temperature (K)	296	
D_c (g cm^{-3})	1.630	1.593
μ (mm^{-1})	1.10	1.33
θ range (°)	3.2-26.4	3.5-26.5
Measured refls.	17755	17602
Independent refls.	3844	3147
R_{int}	0.040	0.068
S	1.13	1.12
R1/wR2	0.050/0.103	0.081/0.173
$\Delta\rho_{max}/\Delta\rho_{min}$ (eÅ^{-3})	0.35/-0.33	0.58/-0.55

Table 2
Selected bond distances (Å, °).

Fe1			
Fe1-O1	1.897(2)	Fe1-O3	1.907(2)
Fe1-N1	2.067(3)	Fe1-N3	2.076(3)
Fe1-Cl1	2.2146(11)		
O1-Fe1-O3	92.51(10)	O1-Fe1-N1	87.07(10)
O3-Fe1-N1	144.71(11)	O1-Fe1-N3	147.74(11)
O3-Fe1-N3	87.47(11)	N1-Fe1-N3	74.99(11)
O1-Fe1-Cl1	108.50(8)	O3-Fe1-Cl1	108.66(9)
N1-Fe1-Cl1	104.86(8)	N3-Fe1-Cl1	102.00(9)
Ni1			
N1-Ni1	1.842(6)	N3-Ni1	1.839(6)
Ni1-O1	1.842(5)	Ni1-O3	1.873(5)
N3- Ni1-O1	178.7(3)	N3-Ni1-N1	83.6(3)
O1-Ni1-N1	95.3(2)	N3-Ni1-O3	94.5(2)
O1-Ni1-O3	86.6(2)	N1-Ni1-O3	178.0(2)

Table 3
Hydrogen bond parameters (Å, °).

D-H•••A	D-H	H•••A	D•••A	D-H•••A
Fe1				
C4—H4•••F1^{i}	0.93	2.45	3.249 (12)	146
Ni1				
C4—H4•••O4^{i}	0.93	2.53	3.408 (9)	159

Symmetry code: (i) x, y, z+1 for **Fe1**; (i) x+1, y+1, z for **Ni1**.

the diffraction patterns of complexes given in Figures S6 and S7 which reveals crystalline nature of the complexes.

The Miller indices (hkl) along with observed and calculated d angles, 2θ values, and relative intensities are given in Table S3. The average crystalline sizes of the complexes were calculated using Debye Scherrer equation (D = K λ / β Cos θ) Where D = Particle size, K = Dimensionless shape factor, λ = X-ray wavelength (1.5406 Å) β = full width at half maximum of the diffraction peak, θ = Diffraction angle. The complexes of **Fe1-Ni1** have a crystalline size of 32.09 for **Fe1** and 47.63 nm for **Ni1** respectively suggesting that the complexes are in a nanocrystalline phase.

3.4. Antiviral activity

Serious acute respiratory syndrome coronavirus (SARS-CoV), SARS-CoV2 and the Middle East respiratory syndrome coronavirus (MERS-CoV) have caused fatal outbreaks of pneumonia. Other members of the Coronaviridae family of zoonotic origin are endemic in the human population and account for up to 30% of mild respiratory infections [43–46]. The discovery of new inhibitors that can be used in the treatment of viral diseases, including Covid-19, is an area open to research, and there is a need for innovative compounds with increased efficiency that provide inhibition by suppressing enzyme, and receptor mechanisms.

Although there are studies showing that different thiosemicarbazone compounds have antiviral effects, there are limited studies on their antiviral effects against the SARS-CoV2 virus [47,48]. In these studies, the binding affinities against SARS-CoV2 were examined bioinformatically. However, the direct effects of thiosemicarbazone compounds against the SARS-CoV2 virus, natural immunity and cell death caused by inflammation induced by cytokine stimulation are unknown.

To predict the binding affinity and pose of both compounds to the 3C-like protease enzyme specific to the SARS-CoV-2 virus, docking calculations were performed. As a result of the rigid docking calculation the best docking pose docking score estimated to be -7.4 kcal/mol for **Fe1**, and -7.0 kcal/mol for **Ni1**. The residues GLY143 and THR26 backbone have hydrogen bond interaction with **Fe1**. For **Ni1**, similar hydrogen bond interaction was observed with

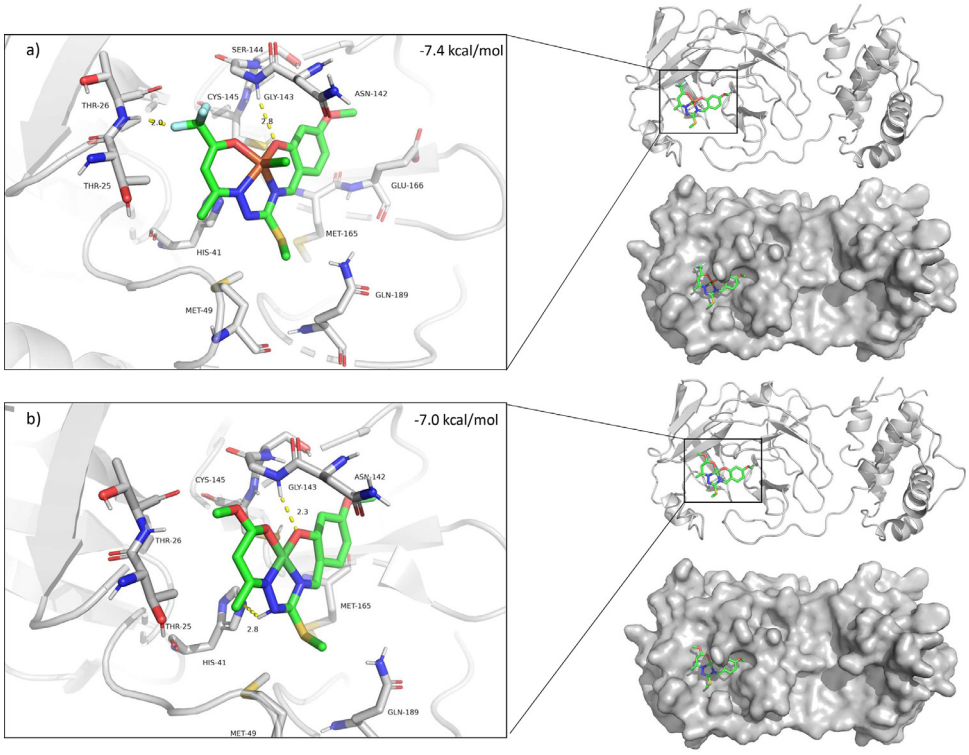

Fig. 3. The best binding pose of molecular rigid docking results of **Fe1 (a)** and **Ni1 (b)**.

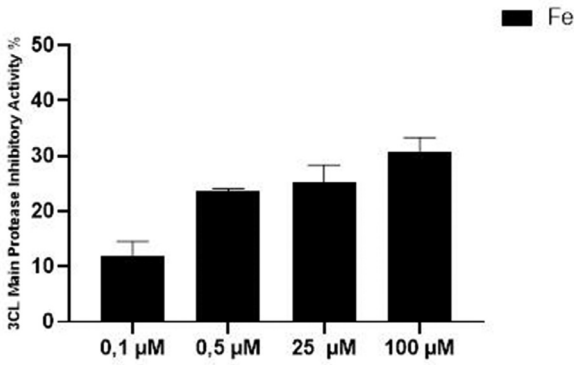

Fig. 4. 3CL main protease inhibitory activity of **Fe1**.

GLY143, and in addition HIS41 is in the range of making hydrogen bond interaction (Fig. 3). Next, in order to assess possible conformations of the residues side chains that may affect binding were selected through manually inspection for flexible docking. As a result of the flexible docking procedure, the highest docking score is -7.8 for both **Fe1** and **Ni1**. It has been observed in **Fe1** binding pose that ASN142 side chain amine group located in between Fe1-O3 and Fe1-Cl atoms, similar position is observed for **Ni1** as well (Figure S5).

In accordance with the results obtained, inhibitory effect of **Fe1** compound showing higher binding affinity against SARS-CoV-2 virus specific 3C-like protease enzyme was investigated experimentally. It was determined that the highest inhibition concentration of **Fe1** compound was 100 μM. Percent inhibition activity at this concentration was on average 30.62 $\pm$ 3.809% (Fig. 4).

Tang and colleagues, in a randomized controlled study of 150 patients, found that hydroxychloroquine had no significant effect on accelerating viral clearance. Moreover, side effects were observed in patients treated with 800-1200mg of hydroxychloroquine per day compared to patients treated without hydroxychloroquine [49].

In another study, placebo-controlled, randomized remdesivir trials were conducted in patients with Covid-19. It was found that there was no significant difference between the time to clinical recovery in the remdesivir-treated group and the time to recovery in the placebo-treated group. Although the number of patients using remdesivir within 10 days of symptoms onset was higher than in the placebo group, the 28-day mortality was similar for both groups. No significant difference was observed between the two groups in terms of oxygen support duration, length of hospital stay, and clinical recovery rates on the 14th and 28th days [50].

In our previous studies in the context of antiproliferation, it was found that iron(III) complexes of such N_2O_2-chelating thiosemicarbazones are more active than those with other metal ions, nickel(II), manganese(III) etc. [7,8,11]. Experiments with 3 CL-like protease enzyme also confirmed the activity superiority of iron(III) complex

4. Conclusion

The new iron(III) and nickel(II) complexes with N_2O_2-thiosemicarbazones were synthesized and carried out the purity and structural confirmation. The inhibitory effects of the two compounds against SARS-CoV2 3CL-like protease were investigated by experimental and theoretical methods. Complex **Fe1** was more effective than **Ni1** and proved that it can be a potent inhibitor for such enzymes.

The experimental and theoretical results showed once again that the metal specie in such thiosemicarbazone complexes cause significant differences in biological activity. Within the scope of the investigation of antiviral effects iron(III)-thiosemicarbazone complexes, it is obvious that complex Fe1 may be pioneer to achieve the better ones. This study includes the first knowledges related to inhibitory activity of such thiosemicarbazone complexes on 3CL-like protease enzyme.

Supplementary Material: Crystallographic data for the structural analysis have been deposited with the Cambridge Crystallographic Data Centre, CCDC No. 1997452 for **Fe1** and 1997453 for **Ni1**. Copies of this information may be obtained free of charge from the Director, CCDC, 12 Union Road, Cambridge CB2 1EZ, UK (fax: +44-1223-336033; e-mail: deposit@ccdc.cam.ac.uk or www: http://www.ccdc.cam.ac.uk).

Declaration of Competing Interest

The authors declare that they have no known competing financial interests or personal relationships that could have appeared to influence the work reported in this paper.

CRediT authorship contribution statement

Belkis Atasever Arslan: Conceptualization, Methodology, Supervision, Investigation, Visualization, Writing – review & editing. **Büşra Kaya:** Visualization, Investigation, Validation. **Onur Şahin:** Visualization, Investigation, Validation. **Sefer Baday:** Investigation, Formal analysis, Validation. **Cemil Can Saylan:** Investigation, Formal analysis, Validation. **Bahri Ülküseven:** Writing – review & editing, Supervision, Methodology.

Acknowledgements

The authors acknowledge to Scientific and Technological Research Application and Research Center, Sinop University, Turkey, for the use of the Bruker D8-QUEST diffractometer. The authors declare patent application (Turk Patent and Trademark Office, Ref. no. PT2020-22067). There are no further patents, products in development or marketed products to declare.

Supplementary materials

Supplementary material associated with this article can be found, in the online version, at doi:10.1016/j.molstruc.2021.131166.

References

[1] D. Singh, R.V. Singh, Synthetic and biochemical aspects of titanocene- and zirconocene-dichloride chelates of thiosemicarbazones derived from heterocyclic ketones, J. Inorg. Biochem. 15 (1993) 227–234.
[2] M. Baldini, M. Belicchi-Ferrari, F. Bisceglie, P.P. Dall'Aglio, G. Pelosi, S. Pinelli, P. Tarasconi, Copper(II) Complexes with Substituted Thiosemicarbazones of α-Ketoglutaric Acid: synthesis, X-ray Structures, DNA Binding Stud., Nuclease Biol. Activity 43 (2004) 7170–7179 Inorganic Chemistry.
[3] F. Trudu, F. Amato, P. Vaňhara, T. Pivetta, E.M. Peña-Méndez, J. Havel, Coordination compounds in cancer: past, present and perspectives, J. Appl. Biomed. 13 (2015) 79–103.
[4] D. Kovala-Demertzi, M.A. Demertzis, J.R. Miller, C. Papadopoulou, C. Dodorou, G. Filousis, Platinum(II) complexes with 2-acetyl pyridine thiosemicarbazone: synthesis, crystal structure, spectral properties, antimicrobial and antitumour activity, J. Inorg. Biochem. 86 (2001) 555–563.
[5] A. Garoufis, S.K. Hadjikakou, N. Hadjiliadis, Palladium coordination compounds as anti-viral, anti-fungal, anti-microbial and anti-tumor agents, Coord. Chem. Rev. 253 (2009) 1384–1397.
[6] D. Özerkan, O. Ertik, B. Kaya, S. Erdem Kuruca, R. Yanardag, B. Ülküseven, Novel palladium (II) complexes with tetradentate thiosemicarbazones. Synthesis, characterization, in vitro cytotoxicity and xanthine oxidase inhibition, Invest. New Drugs 37 (2019) 1187–1197.
[7] B. Atasever, B. Ülküseven, T. Bal-Demirci, S. Erdem-Kuruca, Z. Solakoğlu, Cytotoxic activities of new iron(III) and nickel(II) chelates of some S-methyl-thiosemicarbazones on K562 and ECV304 cells, Invest. New Drugs 28 (2010) 421–432.
[8] T. Bal-Demirci, G. Congur, A. Erdem, S. Erdem-Kuruca, N. Özdemir, K. Akgün–Dar, B. Varol, B. Ülküseven, Iron(III) and nickel(II) complexes as potential anticancer agents: synthesis, physicochemical and structural properties, cytotoxic activity and DNA interactions, New J. Chem. 39 (2015) 5643.
[9] B. Kaya, B. Atasever-Arslan, Z. Kalkan, H. Gür, B. Ülküseven, Apoptotic mechanisms of nickel (II) complex with *N*1-acetylacetone-*N*4-4-methoxy-salicylidene-*S*-allyl-thiosemicarbazone on HL60 leukemia cells, Gen. Physiol. Biophys. 35 (2016) 451–458.
[10] M. Süleymanoğlu, B. Kaya, S. Erdem-Kuruca, B. Ülküseven, Iron(III) and nickel(II) complexes of tetradentate thiosemicarbazones: Synthesis, atructure, cytotoxicity, and lipophilicity, J. Biochem. Mol. Toxicol. (2019) 22383.
[11] B. Kaya, Z.K. Yılmaz, O. Şahin, B. Aslim, Ü. Tükenmez, B. Ülküseven, Structural analysis and biological functionalities of iron(III)-and manganese(III)-thiosemicarbazone complexes: in vitro anti–proliferative activity on human cancer cells, DNA binding and cleavage studies, J. Biol. Inorg. Chem. 24 (2019) 365–376.
[12] R. Yanardag, T. Bal Demirci, B. Ulkuseven, S. Bolkent, S. Tunalı, S. Bolkent, Synthesis, characterization and antidiabetic properties of N(1)-2,4-dihydroxybenzylidene-N(4)-2-hydroxybenzylidene-S-methyl-thiosemicarbazidato-oxovanadium(IV), Eur. J. Med. Chem. 44 (2009) 818–826.
[13] B.İ. Ceylan, A. Yilmaz, O. Bölükbaşı, E. Türker Acar, M. Özyürek, Y. Kurt, B. Ülküseven, A square-pyramidal iron(III) complex obtained from 2-hydroxy-benzophenone-S-allylthiosemicarbazone: Synthesis, characterization, electrochemistry, quantum chemical studies and antioxidant capability, J. Coordination Chem., 73 NO 1 (2020) 120–136.
[14] T. Bal-Demirci, M. Şahin, M. Özyürek, E. Kondakçı, B. Ülküseven, Synthesis, antioxidant activities of the nickel (II), iron (III) and oxovanadium (IV) complexes with N2O2 chelating thiosemicarbazones, Spectrochim. Acta, Part A 126 (2014) 317.
[15] B. Kaya, O. Şahin, M. Bener, B. Ülküseven, Iron (III) and nickel (II) complexes with S-alkyl (n-C1-6)-thiosemicarbazidato ligands: Synthesis, structural characterization, and antioxidant features, J. Mol. Struct. 1167 (2018) 16.
[16] E. Petersen, M. Koopmans, U. Go, D.H. Hamer, N. Petrosillo, F. Castelli, M. Storgaard, S. Al Khalili, L. Simonsen, Comparing SARS-CoV-2 with SARS-CoV and influenza pandemics, Lancet Infect. Dis. 20 (2020) e238–e244.
[17] JE. Crowe, Host Defense Mechanisms Against Viruses, in: Fetal and Neonata Physiology. Fifth Edition, 2017, pp. 1175–1197.
[18] J.R. Tisoncik, M.J. Korth, C.P. Simmons, J. Farrar, T.R. Martin, MG. Katze, Into the eye of the cytokine storm, Microbiol. Mol. Biol. Rev. 76 (2012) 16–32.
[19] R. Karki, B.R. Sharma, S. Tuladhar, E.P. Williams, L. Zalduondo, P. Samir, M. Zheng, B. Sundaram, B. Banoth, R.K.S. Malireddi, P. Schreiner, G. Neale, P. Vogel, R. Webby, C.B. Jonsson, TD. Kanneganti, Synergism of TNF-α and IFN-γ Triggers Inflammatory Cell Death, Tissue Damage, and Mortality in SARS-CoV-2 Infection and Cytokine Shock Syndromes, Cell. 184 (1) (2021) 149–168.
[20] D. Palanimuthu, S.V. Shinde, K. Somasundaram, AG. Samuelson, In vitro and in vivo anticancer activity of copper bis(thiosemicarbazone) complexes, J. Med. Chem. 56 (2013) 722–734.
[21] A.S. Khan, M. Yusuf, Synthesis, spectral studies and in vitro antibacterial activity of steroidal thiosemicarbazone and their palladium(II) complexes, Eur. J. Med. Chem. 44 (2009) 2270–2274.
[22] M. Karatepe, F. Karatas, Antioxidant, pro-oxidant effect of the thiosemicarbazone derivative Schiff base (4-(1-phenylmethylcyclobutane-3-yl)-2-(2-hydroxy-benzylidenehydrazino) thiazole) and its metal complexes on rats, Cell Biochem. Funct. 24 (2006) 547–554.
[23] S. Padhye, Z. Afrasiabi, E. Sinn, J. Fok, K. Mehta, N. Rath, Antitumor metallothiosemicarbazonates: structure and antitumor activity of palladium complex of phenanthrenequinone thiosemicarbazone, Inorg. Chem. 44 (2005) 1154–1156.
[24] A.P. Rebolledo, M. Vieites, D. Gambino, O.E. Piro, E.E. Castellano, C.L. Zani, E.M. Souza-Fagundes, L.R. Teixeira, A.A. Batista, H. Beraldo, Palladium(II) complexes of 2-benzoylpyridine-derived thiosemicarbazones: spectral characterization, structural studies and cytotoxic activity, J. Inorg. Biochem. 99 (2005) 698–706.
[25] I.H. Hall, C.B. Lackey, T.D. Kistler, Durh.am RWJr, E.M. Jouad, M. Khan, X.D. Thanh, S. Djebbar-Sid, O. Benali-Baitich, GM. Bouet, Cytotoxicity of copper and cobalt complexes of furfural semicarbazone and thiosemicarbazone derivatives in murine and human tumor cell lines, Pharmazie 55 (2000) 937–941.
[26] A.E. Stacy, D. Palanimuthu, P.V. Bernhardt, D.S. Kalinowski, P.J. Jansson, DR. Richardson, Zinc(II)-Thiosemicarbazone Complexes Are Localized to the Lysosomal Compartment Where They Transmetallate with Copper Ions to Induce Cytotoxicity, J. Med. Chem. 59 (2016) 4965–4984.
[27] A. Karaküçük-İyidoğan, D. Taşdemir, E.E. Oruç-Emre, J. Balzarini, Novel platinum (II) and palladium (II) complexes of thiosemicarbazones derived from 5-substitutedthiophene-2-carboxaldehydes and their antiviral and cytotoxic activities, Eur. J. Med. Chem. 46 (2011) 5616–5624.
[28] T. Varadinova, D. Kovala-Demertzi, M. Rupelieva, M. Demertzis, P. Genova, Antiviral activity of platinum(II) and palladium(II) complexes of pyridine-2-carbaldehyde thiosemicarbazone, Acta Virol. 45 (2001) 87–94.
[29] G. Pelosi, F. Bisceglie, F. Bignami, P. Ronzi, P. Schiavone, M.C. Re, C. Casoli, E.J. Pilotti, Antiretroviral Activity of Thiosemicarbazone Metal Complexes, Med. Chem. 53 (24) (2010) 8765–8769.
[30] T. Bal, B. Atasever, Z. Solakoğlu, S. Erdem-Kuruca, B. Ülküseven, Synthesis, characterisation and cytotoxic properties of the N1, N4-diarylidene-S-methyl-thiosemicarbazone chelates with Fe (III) and Ni (II), Eur. J. Med. Chem. 42 (2) (2007) 161–167.
[31] A.A.A. Abdusalam, V. Murugaiyah, Identification of Potential Inhibitors of 3CL Protease of SARS-CoV-2 From ZINC Database by Molecular Docking-Based Virtual Screening, Front. Mol. Biosci. 17 (7) (2020) 603037 2020.
[32] G.M. Sheldrick, A short history of SHELX, Acta Cryst. A64 (2008) 112.
[33] G.M. Sheldrick, Crystal structure refinement with SHELXL, Acta Cryst. C71 (2015) 3.
[34] APEX2, Bruker AXS Inc. Madison Wisconsin USA (2013).

[35] C.F. Macrae, I. Sovago, S.J. Cottrell, P.T.A. Galek, P. McCabe, E. Pidcock, M. Platings, G.P. Shields, J.S. Stevens, M. Towler, P.A. Wood, J. Appl. Cryst. 53 (2020) 226–235.
[36] L.J. Farrugia, J. Appl. Cryst. 45 (2012) 849–854.
[37] C. Yamazaki, J. Chem. 53 (1975) 610–615.
[38] J. Gradinaru, A. Forni, Y. Simonov, M. Popovici, S. Zecchin, M. Gdaniec, D.E. Fenton, Inorg. Chim. Acta 357 (2004) 2728–2736.
[39] B. Kaya, B. Ülküseven, O. Şahin, Z.S. Şahin, J. Mol. Struct. 1191 (2019) 337–344.
[40] O. Trott, AJ. Olson, AutoDock Vina: improving the speed and accuracy of docking with a new scoring function, efficient optimization, and multithreading, J. Comput. Chem. 31 (2) (2010) 455–461.
[41] T.J. Dolinsky, P. Czodrowski, H. Li, J.E. Nielsen, J.H. Jensen, G. Klebe, NA. Baker, PDB2PQR: expanding and upgrading automated preparation of biomolecular structures for molecular simulations, Nucleic Acids Res. 35 (suppl_2) (2007) W522–W525.
[42] Seo S., Park J.W., An D., Yoon J., Paik H., & Hwang S. (2020). Supercomputer-aided Drug Repositioning at Scale: Virtual Screening for SARS-CoV-2 Protease Inhibitor. Under review in DTMBIO.
[43] B.A. Arslan, AC. Timucin, Immunotherapy approaches on innate immunity for SARS-Cov-2, Acta Virol. 64 (4) (2020) 389–395.
[44] M. Hoffmann, H. Kleine-Weber, S. Schroeder, N. Krüger, T. Herrler, S. Erichsen, T.S. Schiergens, G. Herrler, N.H. Wu, A. Nitsche, M.A. Müller, C. Drosten, S. Pöhlmann, SARS-CoV-2 Cell Entry Depends on ACE2 and TMPRSS2 and Is Blocked by a Clinically Proven Protease Inhibitor, Cell. 181 (2020) 271–280 .e8.
[45] X. Ou, Y. Liu, X. Lei, P. Li, D. Mi, L. Ren, L. Guo, R. Guo, T. Chen, J. Hu, Z. Xiang, Z. Mu, X. Chen, J. Chen, K. Hu, Q. Jin, J. Wang, Z. Qian, Characterization of spike glycoprotein of SARS-CoV-2 on virus entry and its immune cross-reactivity with SARS-CoV, Nat. Commun. 11 (2020) 1620.
[46] M.A. Tortorici, A.C. Walls, Y. Lang, C. Wang, Z. Li, D. Koerhuis, G.J. Boons, B.J. Bosch, F.A. Rey, R.J. de Groot, D. Veesler, Structural basis for human coronavirus attachment to sialic acid receptors, Nat. Struct. Mol. Biol. 26 (2019) 481–489.
[47] J. Haribabu, S. Srividya, D. Mahendiran, D. Gayathri, V. Venkatramu, N. Bhuvanesh, R. Karvembu, Synthesis of Palladium(II) Complexes via Michael Addition: Antiproliferative Effects through ROS-Mediated Mitochondrial Apoptosis and Docking with SARS-CoV-2, Inorg. Chem. 59 (23) (2020) 17109–17122.
[48] M. Haroon, T. Akhtar, M. Khalid, S. Ali, S. Zahra, I. Ul Haq, M. Alhujaily, Synthesis, antioxidant, antimicrobial and antiviral docking studies of ethyl 2-(2-(arylidene)hydrazinyl)thiazole-4-carboxylates, J Biosci. (2021) Apr 26, doi:10.1515/znc-2021-0042.
[49] W. Tang, Z. Cao, M. Han, Z. Wang, J. Chen, W. Sun, Y. Wu, W. Xiao, S. Liu, E. Chen, W. Chen, X. Wang, J. Yang, J. Lin, Q. Zhao, Y. Yan, Z. Xie, D. Li, Y. Yang, L. Liu, J. Qu, G. Ning, G. Shi, Q. Xie, Hydroxychloroquine in patients with mainly mild to moderate coronavirus disease 2019: open label, randomised controlled trial, BMJ 369 (2020) m1849.
[50] Y. Wang, D. Zhang, G. Du, R. Du, J. Zhao, Y. Jin, S. Fu, L. Gao, Z. Cheng, Q. Lu, Y. Hu, G. Luo, K. Wang, Y. Lu, H. Li, S. Wang, S. Ruan, C. Yang, C. Mei, Y. Wang, D. Ding, F. Wu, X. Tang, X. Ye, Y. Ye, B. Liu, J. Yang, W. Yin, A. Wang, G. Fan, F. Zhou, Z. Liu, X. Gu, J. Xu, L. Shang, Y. Zhang, L. Cao, T. Guo, Y. Wan, H. Qin, Y. Jiang, T. Jaki, F.G. Hayden, P.W. Horby, B. Cao, C. Wang, Remdesivir in adults with severe COVID-19: a randomised, double-blind, placebo-controlled, multicentre trial, Lancet. 395 (10236) (2020) 1569–1578.